Tectonics

RESEARCH ARTICLE
10.1029/2022TC007344

Late Miocene Exhumation of the Western Cordillera, Ecuador, Driven by Increased Coupling Between the Subducting Carnegie Ridge and the South American Continent

Audrey Margirier[1,2,3], Manfred R. Strecker[1], Peter W. Reiners[2], Stuart N. Thomson[2], Ismael Casado[1], Sarah W. M. George[2,4], and Alexandra Alvarado[5]

[1]Institut für Geowissenschaften, Universität Potsdam, Potsdam, Germany, [2]Department of Geosciences, University of Arizona, Tucson, AZ, USA, [3]Now at the Institute of Earth Surface Dynamics, University of Lausanne, Lausanne, Switzerland, [4]School of Geology and Geophysics, University of Oklahoma, Norman, OK, USA, [5]Instituto Geofísico, Escuela Politécnica Nacional, Quito, Ecuador

Abstract The subduction of bathymetric highs, such as aseismic ridges, leads to far-reaching changes in the dynamics of subduction zones with increased plate coupling and deformation in the upper plate. Subduction of the submarine Carnegie Ridge on the Nazca Plate has fundamentally impacted late Cenozoic magmatism and tectonic activity in the northern Andes. However, the timing of onset of Carnegie Ridge subduction has been a matter of debate. Time-temperature inverse modeling of new thermochronological data from the Western Cordillera of Ecuador reveals two phases of cooling separated by isothermal conditions. The first cooling phase postdates early and middle Miocene magmatism in the Western Cordillera and is attributed to post-magmatic thermal relaxation. The second cooling phase started after 6 Ma. Inferred to record the onset of tectonically controlled rock uplift and exhumation in the Western Cordillera, this phase is coeval with the last cooling phase recorded in the Eastern Cordillera. Based on these findings, we suggest that the onset of subduction of the Carnegie Ridge at ~6–5 Ma increased plate coupling at the subduction interface, promoting shortening, regional rock uplift, and exhumation in the northern Andes. Overall, our results highlight the essential role of bathymetric highs in driving regional upper-plate deformation at non-collisional convergent plate margins.

Plain Language Summary Topographic growth and morphology of the Andes have been influenced by subduction processes, tectonic inheritance, and climate. Here, we investigate the role of subduction of high topography on the ocean floor in driving deformation in the upper plate at the Nazca-South America ocean-continent plate margin. The subduction of the Carnegie Ridge, a linear, topographically high sector on the Nazca Plate, has impacted magmatism and deformation processes in the Ecuadorian Andes. However, the timing of onset of ridge subduction is debated. We employed radioisotopic dating techniques to evaluate the uplift of the Andes. These techniques record the cooling of rocks as mountain ranges are uplifted and eroded. The thermal histories of rocks from the Western Cordillera in Ecuador reveal two distinct cooling phases. The first cooling phase occurred shortly after Miocene magmatic bodies were emplaced in the Western Cordillera. The second cooling phase began at ~6–5 Ma, coeval with the last cooling phase in the Eastern Cordillera. We attribute this cooling phase to the onset of uplift and erosion in the Western Cordillera. Based on these findings, we suggest that the onset of subduction of the Carnegie Ridge increased plate coupling and promoted shortening and rock uplift in the northern Andes.

Key Points:

- Thermochronological data reveal two cooling phases in the Western Cordillera of Ecuador, during the Miocene and after 6 Ma
- The onset of cooling at 6 Ma was associated with shortening, rock uplift, and exhumation in the Western Cordillera
- Mio-Pliocene exhumation was related to stronger coupling of the subduction interface due to the initial subduction of the Carnegie Ridge

Supporting Information:

Supporting Information may be found in the online version of this article.

Correspondence to:

A. Margirier,
audrey.margirier@uni-potsdam.de

Citation:

Margirier, A., Strecker, M. R., Reiners, P. W., Thomson, S. N., Casado, I., George, S. W. M., & Alvarado, A. (2023). Late Miocene exhumation of the Western Cordillera, Ecuador, driven by increased coupling between the subducting Carnegie Ridge and the South American continent. *Tectonics*, *42*, e2022TC007344. https://doi.org/10.1029/2022TC007344

Received 11 APR 2022
Accepted 23 NOV 2022

Author Contributions:

Conceptualization: Audrey Margirier, Manfred R. Strecker
Formal analysis: Audrey Margirier
Funding acquisition: Audrey Margirier, Manfred R. Strecker
Investigation: Audrey Margirier, Stuart N. Thomson, Ismael Casado, Sarah W. M. George
Methodology: Audrey Margirier, Peter W. Reiners, Stuart N. Thomson, Sarah W. M. George

1. Introduction

Subduction of buoyant bathymetric highs, such as aseismic ridges and oceanic plateaus, often results in far-reaching changes in the dynamics of the subduction zone and deformation processes in the upper plate (e.g., Flóres-Rodríguez et al., 2019; Geist et al., 1993; Horton et al., 2022; Rosenbaum & Mo, 2011). The subduction of bathymetric highs is known to increase the coupling at the plate interface (e.g., Das & Watts, 2009; Singh et al., 2011; Taylor et al., 2005) and may result in flat-slab subduction geometries (e.g., Gutscher et al., 1999; Jordán et al., 1983), thus modifying the tectono-magmatic evolution of the overriding plate (e.g., Axen et al., 2018; Gutscher et al., 1999; Margirier et al., 2017; Ramos & Folguera, 2009). For example, field observations and modeling studies suggest that subduction of bathymetric highs enhances upper-plate deformation and promotes regional uplift that propagates away from the trench (e.g., Dominguez et al., 2000; Georgieva et al., 2016; Gerya

Project Administration: Audrey Margirier
Resources: Manfred R. Strecker, Peter W. Reiners, Alexandra Alvarado
Supervision: Manfred R. Strecker, Peter W. Reiners
Visualization: Audrey Margirier
Writing – original draft: Audrey Margirier
Writing – review & editing: Audrey Margirier, Manfred R. Strecker, Peter W. Reiners, Stuart N. Thomson, Sarah W. M. George, Alexandra Alvarado

et al., 2009; Martinod et al., 2013). In addition, aseismic ridge subduction may induce changes in magmatic activity (e.g., Chiarada et al., 2020; Kay & Mpodozis, 2002; Ramos & Kay, 1992; Yang et al., 1996), leading to non-magmatic sectors of volcanic arcs (e.g., Nur & Ben-Avraham, 1981; Pilger, 1981; Rosenbaum & Mo, 2011; Yang et al., 1996). Important changes in the dip of the subducting plate may also have an impact on mantle dynamics and influence dynamic topography of the upper plate (e.g., Dávila et al., 2010; Eakin et al., 2014; Gérault et al., 2015; Liu, 2015). In addition to the subduction of bathymetric anomalies and its impact on upper-plate processes, inherited lithospheric-scale heterogeneities and strength contrasts in the upper plate exert first-order controls on deformation, uplift, and magmatic processes, thus influencing the build-up of topography in subduction orogens (e.g., Horton & Fuentes, 2016; Isacks, 1988; Rodriguez Piceda et al., 2022; Waldien et al., 2022).

The topography and morphology of the Andes are the result of from crustal shortening and thickening associated with the convergence of the oceanic Nazca Plate and the continental South American Plate (e.g., Armijo et al., 2015; Isacks, 1988); in addition, the evolution of this orogen has been significantly influenced by the formation of meridional orographic barriers and superposed asymmetric climate-driven surface processes (e.g., Bookhagen & Strecker, 2008; McQuarrie et al., 2008; Strecker et al., 2007; Thomson et al., 2010). Along the coastal sectors of the South American continental margin, the subduction of bathymetric anomalies is mirrored by differential coastal uplift and the distribution of marine terraces (e.g., Freisleben et al., 2021; Gardner et al., 1992; Hsu, 1992; Macharé & Ortlieb, 1992; Pedoja et al., 2006; Saillard et al., 2011). On larger spatial scales involving the orogen interior and the foreland, distributed deformation and range uplifts in the broken foreland and the evolution of non-magmatic sectors are also thought to have resulted from strong plate coupling associated with the subduction of bathymetric anomalies (e.g., Giambiagi et al., 2012; Horton & Fuentes, 2016; Ramos & Folguera, 2009). For example, the broken-foreland uplifts of the Andean foreland and the non-magmatic arc segment in Argentina have been linked to flat-slab subduction (e.g., Capaldi et al., 2020; Jordán et al., 1983; Kay et al., 1987; Ramos et al., 2002). Furthermore, long-wavelength uplift of the Amazonian foreland is thought to reflect basal shear and thickening of the lower crust associated with the subduction of the Nazca Ridge (e.g., Bishop et al., 2018; Espurt et al., 2010). While the influence of aseismic ridge subduction in the forearc and foreland regions is reasonably well documented, the influence of ridge subduction with respect to the high-elevation regions of the northern Andes has remained uncertain. Some authors suggest that the subduction of the Nazca Ridge and subsequent slab flattening triggered regional uplift in the Western Cordillera and the sub-Andean ranges of northern Peru (e.g., Bishop et al., 2018; George et al., 2023; Margirier et al., 2015); similarly, other authors have linked uplift and exhumation of the Eastern Cordillera in Ecuador and Colombia to ridge subduction (Spikings et al., 2001, 2010; Spikings & Simpson, 2014). However, owing to pulses of shortening unrelated to ridge subduction in the eastern Andes (e.g., Mégard, 1984; Sébrier et al., 1988), an unambiguous link between exhumation and ridge subduction in the northern Andes does not exist.

The oblique subduction of the aseismic Carnegie Ridge in Ecuador (Figure 1a) has strongly influenced the geological evolution of the northern Andes by promoting strike-slip faulting and the northward motion of the North Andean Sliver, reactivating inherited tectonic structures (e.g., Egbue & Kellogg, 2010; Schütt & Whipp, 2020), and driving compositional changes in magmatism (e.g., Barberi et al., 1988; Bourdon et al., 2003; Chiaradia et al., 2020). Strike-slip motion of the North Andean Sliver is mostly accommodated by the Puna-Pallatanga-Cosanga-Chingual fault system (Figure 1b), which has been active at least since the Miocene (e.g., Alvarado et al., 2016; Dumont et al., 2005). Despite its importance for the evolution of the northern Andes, neither the timing of Carnegie Ridge subduction nor its potential impact on uplift and exhumation are well constrained. To unravel these complex relationships between the subducting slab and upper-plate deformation, we integrate new geochronological and thermochronological data from the Western Cordillera with published structural information (e.g., Daly, 1989; Eguez et al., 2003), geochemistry (e.g., Bourdon et al., 2003; George et al., 2021), and existing thermochronological data (Spikings & Crowhurst, 2004; Spikings et al., 2000, 2001, 2010; Winkler et al., 2005) with the principal aim of deciphering the timing of the onset of Carnegie Ridge subduction, its effect on deformation of the South American Plate, and the spatiotemporal patterns of exhumation above and inboard of the subducted portions of the Carnegie Ridge.

2. Geologic and Geodynamic Setting

2.1. Cenozoic Tectonics and Exhumation History of the Ecuadorian Andes

The Ecuadorian Andes constitute a bivergent orogen with active thrusting at the western flank of the Western Cordillera (Eguez et al., 2003; Jaillard et al., 2004, 2005) and in the sub-Andean ranges in the east (Baby et al., 2013).

10.1029/2022TC007344

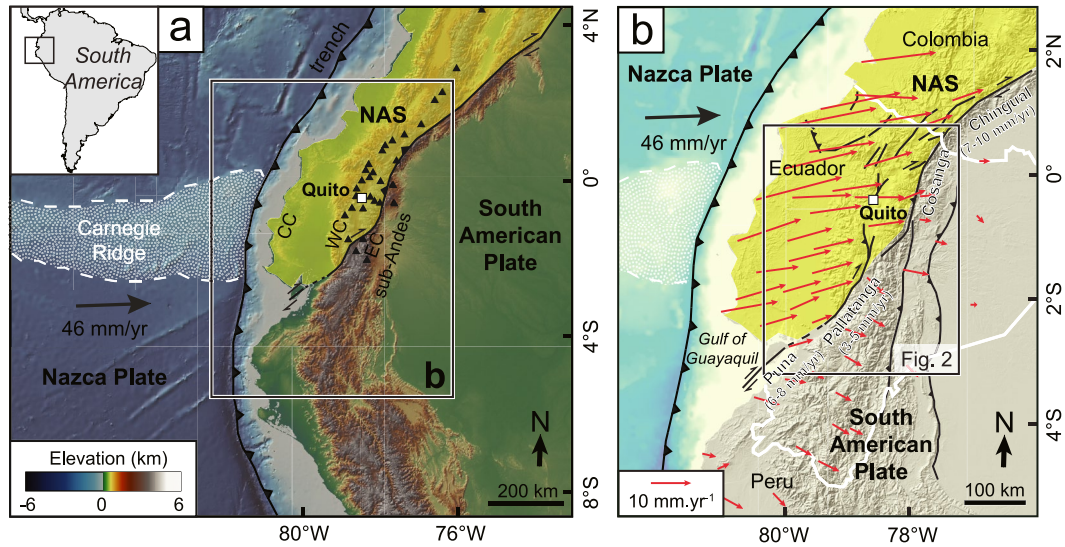

Figure 1. (a) Geodynamic setting and topography of the Ecuadorian Andes with Nazca-Plate bathymetry and Carnegie Ridge. The extent of the North Andean Sliver (NAS) is highlighted in yellow; the Quaternary active volcanoes are indicated by black triangles (Global Volcanism Program, 2022). The Coastal Cordillera (CC), the Western Cordillera (WC), and the Eastern Cordillera (EC) are shown. The inset shows the location of the study area. (b) Principal active faults (black lines; Alvarado et al., 2016) and Global Positioning System horizontal velocity field with respect to stable South America (indicated by red arrows; Nocquet et al., 2014). Quaternary horizontal displacement rates along the different segments of the Puna-Pallatanga-Cosanga-Chingual fault system are indicated below the name of each segment (Baize et al., 2015; Dumont et al., 2005; Ego, 1995; Tibaldi et al., 2007; Winter et al., 1993).

Currently, transpression dominates this region, which causes the northward extrusion of the North Andean Sliver along the dextral Puna-Pallatanga-Cosanga-Chingual fault system (Figure 1b; e.g., Alvarado et al., 2016). The Cosanga fault segment of this deformation zone is mainly characterized by reverse offsets (Alvarado et al., 2016). Quaternary horizontal slip rates along the other segments of the Puna-Pallatanga-Cosanga-Chingual fault system range from 2.5 to 10 mm/yr (Figure 1b; Baize et al., 2015; Dumont et al., 2005; Ego, 1995; Tibaldi et al., 2007; Winter et al., 1993). Northward motion of the North Andean Sliver may have initiated as early as 15 Ma due to oblique subduction of the Nazca Plate (e.g., Alvarado et al., 2016); however, increased coupling at the plate interface after the subduction of the Carnegie Ridge may have caused the acceleration of northward motion of this block as recently as the Pliocene to early Pleistocene (Deniaud, 1999; Witt et al., 2006). Shortening in Ecuador is accommodated by an east-verging fold-and-thrust belt in the Eastern Cordillera and the sub-Andean ranges (Figure 2a; Eguez et al., 2003). Reverse faults along the western flank of the Andes control the uplift of the Western Cordillera and involve Quaternary deposits (Eguez et al., 2003). The Montalvo and the Quinsaloma reverse faults, and the Naranjal and the Ponce Enríquez reverse faults control the uplift of the Western Cordillera north and south of the Puna-Pallatanga-Cosanga-Chingual fault system, respectively (Figures 2c and 2d; Eguez et al., 2003).

The Western and Eastern Cordilleras are separated by the inter-Andean Valley (Figures 1 and 2a), which is filled with Cenozoic volcanic and sedimentary rocks (e.g., Hungerbühler et al., 2002). The Western Cordillera is characterized by a high-elevation (3,500 m), low-relief surface capped by Quaternary volcano-sedimentary deposits and Quaternary volcanoes. The western flank of the Western Cordillera is incised by ∼2-km-deep valleys exposing Oligocene and Miocene intrusions (31–7 Ma; Schütte et al., 2010) and Cretaceous and Paleogene volcano-sedimentary rocks. None of the existing thermochronological data (e.g., Spikings et al., 2005; Winkler et al., 2005, Figure 2a) has resolved the most recent exhumation history of the Western Cordillera that was associated with topographic growth and valley incision on its western flank. Thermochronological data from the Western and Eastern Cordilleras record cooling phases at ∼65–55 and 43–30 Ma that were associated with Cenozoic accretion events and changes in plate kinematics that led to exhumation (e.g., Spikings et al., 2001). Thermochronological data from the Eastern Cordillera also record several exhumation phases from 15 Ma to the present that have been linked to the onset of Carnegie Ridge subduction and to the subduction of a bathymetric high along the subducting ridge (Spikings & Crowhurst, 2004; Spikings et al., 2000, 2001, 2010).

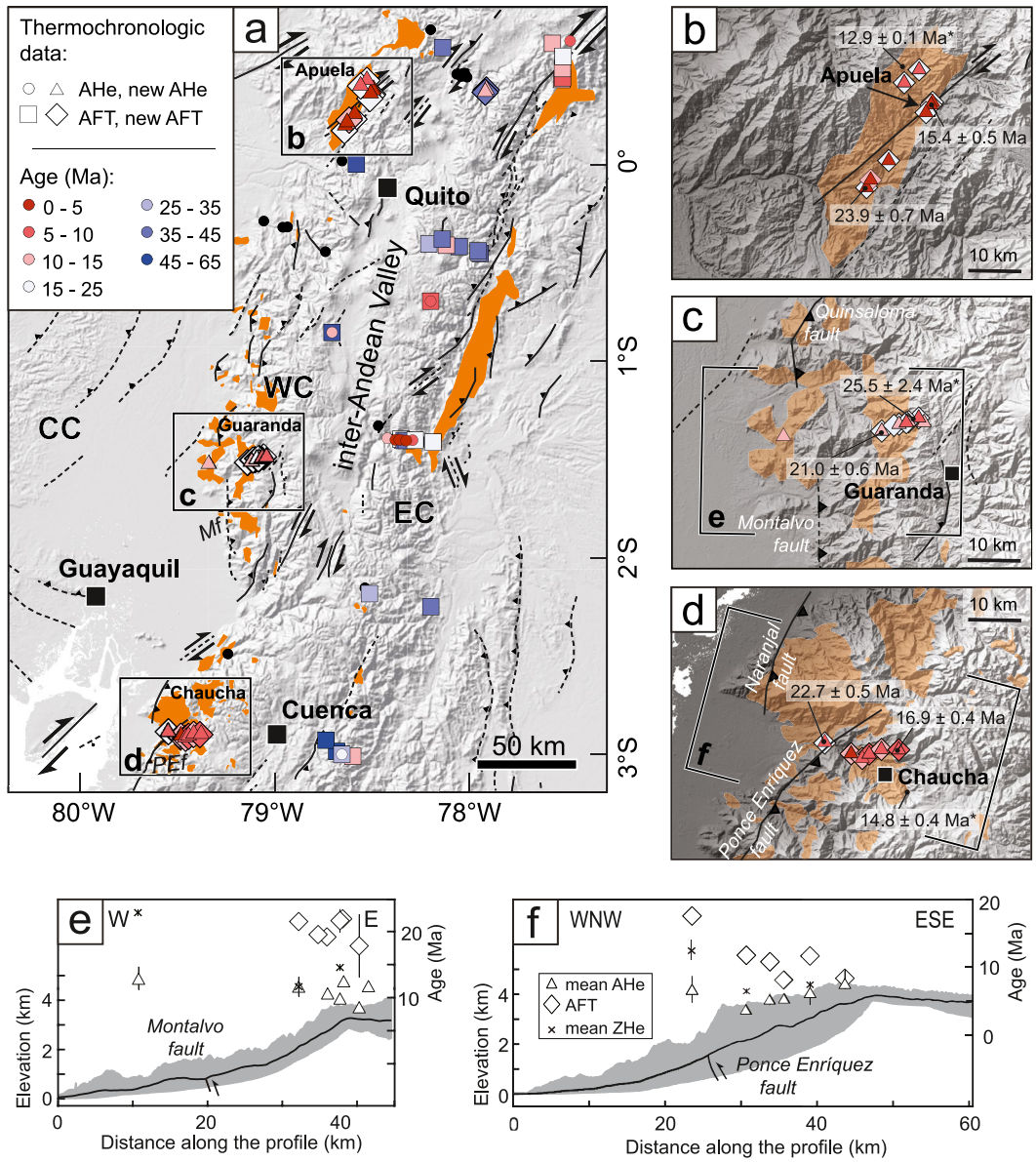

Figure 2. (a) Topographic map showing published, and new thermochronological data from the Ecuadorian Andes (non-reset AHe and AFT ages and volcanism ages indicated by black dots; Spikings & Crowhurst, 2004; Spikings et al., 2000, 2001, 2010; Winkler et al., 2005); intrusions (orange) and faults (Eguez et al., 2003). The Coastal Cordillera (CC), the Western Cordillera (WC), the Eastern Cordillera (EC), the Montalvo fault (Mf), and the Ponce Enríquez fault (PEf) are indicated. (b–d) Detailed views of the Apuela, Guaranda and Chaucha regions with new thermochronological data, intrusions, and faults. Zircon U-Pb ages of the intrusions are indicated on the maps, asterisks indicate ages from Schütte et al. (2010). (e, f) Swath profiles across the Montalvo and the Ponce Enríquez reverse faults, respectively, and thermochronological ages (Guaranda and Chaucha profiles). The error bars are smaller than the symbols for most of the ages.

2.2. Subduction of the Carnegie Ridge

The aseismic Carnegie Ridge is 200 km wide and rises up to 2 km above the surrounding ocean floor (Figure 1); it is one of the most prominent bathymetric highs intercepting the South American trench. Subduction earthquake locations suggest that the Carnegie Ridge is buoyant (e.g., Gutscher et al., 1999). Surface displacements recorded by Global Positioning System during the interseismic phase suggest that the subduction interface between the Carnegie Ridge and the South American Plate is strongly coupled between the surface and 40 km depth (e.g., Chlieh et al., 2014; Nocquet et al., 2014, 2017), although the degree of coupling decreases southward (e.g., Yepes et al., 2016). The oblique subduction of the Carnegie Ridge in Ecuador (Figure 1) is linked with coastal deformation and uplift

(Pedoja et al., 2006), strike-slip faulting (Figure 1; e.g., Alvarado et al., 2016; Baize et al., 2015; Egbue & Kellogg, 2010), changes in magmatism (e.g., Barberi et al., 1988; Bourdon et al., 2003; Chiaradia et al., 2020), and the extrusion of the North Andean Sliver, which is coeval with the opening of the Gulf of Guayaquil (Daly, 1989; Witt & Bourgois, 2010; Witt et al., 2006). However, the timing of onset of Carnegie Ridge subduction is controversial (e.g., Michaud et al., 2009). Spikings et al. (2000, 2001) and Spikings and Crowhurst (2004) suggested an early onset of Carnegie Ridge subduction at 15–10 Ma based on the exhumation history of the Eastern Cordillera. Similarly, based on a plate-kinematic reconstruction, Pilger (1984) proposed that the Carnegie Ridge collided at 15 Ma. In contrast, using a refined plate-kinematic reconstruction, Daly (1989) posited a late Miocene (~8 Ma) onset of Carnegie Ridge subduction, which was thought to be in agreement with the timing of arc widening and migration (e.g., Gutscher et al., 1999), while studies based on the timing of submarine canyon incision, marine terrace uplift, and variation in the spatial distribution and chemistry of magmatism indicated an onset at ~5 Ma (Barberi et al., 1988; Bourdon et al., 2003; Collot et al., 2019; Pedoja et al., 2006). A Pleistocene onset of Carnegie Ridge subduction was suggested based on plate-kinematic reconstructions (Lonsdale & Klitgord, 1978), a shift toward adakitic arc volcanism at 1.5 Ma (Samaniego et al., 2005), and coastal uplift and stratigraphy of marine terraces (Cantalamessa & Di Celma, 2004). In this scenario, the subduction of a bathymetric high was linked with an accelerated escape of the North Andean Sliver (e.g., Hernández et al., 2020; Witt et al., 2006) and concomitant faster subsidence and sedimentation in the Gulf of Guayaquil (Witt et al., 2006).

Given this diversity of interpretations, we aim in this paper not only to resolve the timing of the onset of Carnegie Ridge subduction, but also to decipher its effect on deformation of the South American Plate and to constrain the spatiotemporal patterns of exhumation above and inboard of the subducted portions of the Carnegie Ridge. To do this, we provide new geochronological and thermochronological data from the Western Cordillera to complement published thermochronological data (Spikings & Crowhurst, 2004; Spikings et al., 2000, 2001, 2010; Winkler et al., 2005).

3. Methods

Low-temperature thermochronology records the thermal history of the crust that can be related to exhumation and/or cooling/heating events. Exhumation can be, with supporting geological information, interpreted as the combined result of rock uplift and erosion (e.g., England & Molnar, 1990). Zircon (U-Th)/He (ZHe), apatite fission track (AFT) and apatite (U-Th-Sm)/He (AHe) thermochronometers are sensitive to temperatures ranging from 200°C to 20°C (e.g., Ault et al., 2019). The thermal histories of Chaucha, Guaranda, and Apuela regions in the Western Cordillera (for location refer to Figure 2a) were determined using the QTQt software, which inverts AFT annealing and AHe diffusion parameters for samples with an age-elevation relationship (Gallagher, 2012). We used zircon U-Pb geochronology conducted at the Arizona LaserChron Center and published data (Schütte et al., 2010) to determine the crystallization ages of intrusions and as a constraint for thermal modeling. Additional methodological details can be found in Supplemental Data (Text S1 in Supporting Information S1; Tables S1, S5 and S6 in Supporting Information S2).

4. Results

4.1. Zircon U-Pb Dating

We obtained five new zircon U-Pb ages for the intrusions of the Western Cordillera ranging from 23.9 ± 0.7 to 15.4 ± 0.5 Ma (Figures 2b–2d and 3a–3c; Table 1; Figure S1 in Supporting Information S1, Table S1 in Supporting Information S2). Zircon U-Pb ages from the Apuela Nanegal intrusion in northern Ecuador are 23.9 ± 0.7 (987 m) and 15.4 ± 0.5 Ma (1,676 m). In central Ecuador the zircon U-Pb age of the Telimba Chazo Juan intrusion is 21.0 ± 0.6 Ma (2,086 m). In southern Ecuador the zircon U-Pb ages for the Gaby-Papa Grande intrusion and the Chaucha intrusion are 22.7 ± 0.5 Ma (683 m) and 16.9 ± 0.4 Ma (2,578 m), respectively.

4.2. Low-Temperature Thermochronology

We sampled along two structural cross sections in the central (Guaranda area) and southern parts (Chaucha area) of the Western Cordillera (Figures 2c–2f), spanning an elevation range between 0.9 and 1.4 km. Each transect includes a vertical profile in the hanging wall of the principal reverse fault. We also sampled along a vertical profile in the northern part of the Western Cordillera (Apuela area, Figure 2b).

We present 86 AHe single-grain ages for 22 samples, AFT data for 20 samples, and 26 ZHe single-grain ages for 9 samples (Figure 3; Table 1; Figures S2–S10 in Supporting Information S1; Tables S1–S28 in Supporting

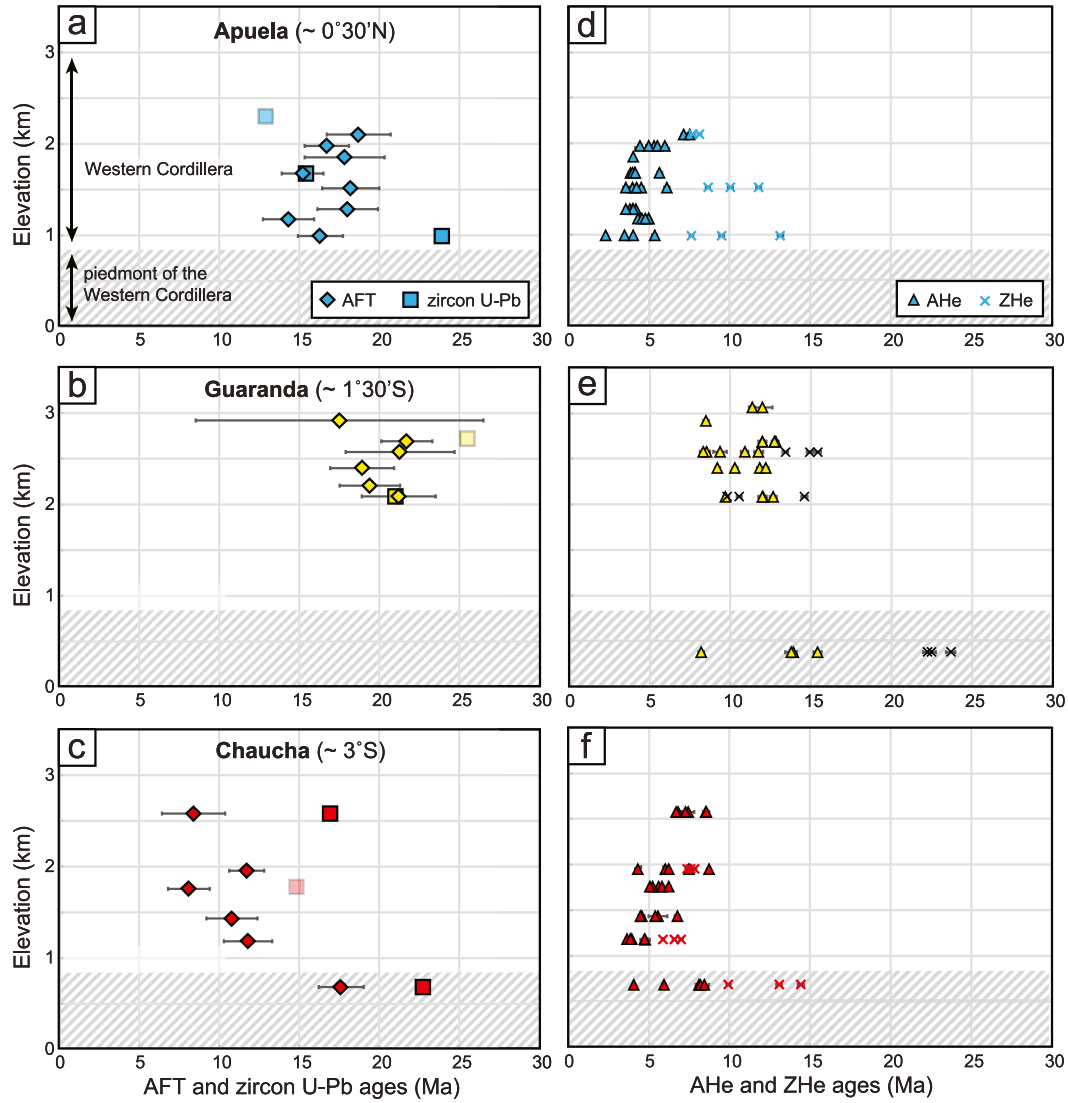

Figure 3. (a–c): New AFT ages and zircon U-Pb ages (data from Schütte et al., 2010 are indicated in pastel colors) from the Western Cordillera plotted against sample elevation for the Apuela, the Guaranda, and the Chaucha profiles. (d–f): New single grain AHe and ZHe ages from the Western Cordillera plotted against sample elevation for the Apuela, the Guaranda, and the Chaucha profiles.

Information S2). AHe single grain ages range from 15.4 ± 0.3 to 2.3 ± 0.1 Ma, AFT ages range from 21.7 ± 1.6 to 8.1 ± 1.3 Ma; mean-track lengths are between 13 and 16 μm. For the same samples ZHe single grain ages are younger than AFT ages and range from 23.6 ± 0.3 to 5.9 ± 0.1 Ma (Figure 3).

Thermochronological ages from the Guaranda cross section are different on either side of the Montalvo reverse fault, with mean AHe and ZHe ages being older in the footwall and younger in the hanging wall (Figure 2e). AFT dates cluster at 20 Ma in the hanging wall and no AFT date is available in the footwall (Figure 2e). Thermochronological ages from the Chaucha cross section record a clear pattern with older AHe, AFT, and ZHe ages for the samples located in the footwall of the Ponce Enríquez reverse fault and younger ages in the hanging wall (Figure 2f).

Combined, the samples from the vertical profiles cover an elevation range from 950 to 3,100 m (Figure 3). Early Miocene AFT ages from the Apuela and Guaranda areas are similar to the plutonic crystallization ages (Figures 3a and 3b). In the Chaucha area, AFT ages cluster at ~11 Ma and are largely invariant with elevation (Figure 3c). AHe ages from the different sampling sites are consistent along the Western Cordillera and show an age-elevation relationship, with a trend toward younger ages at lower elevations (Figures 3d–3f). AHe ages from the Chaucha and Apuela area clearly show a positive age-elevation relationship (Figures 3d and 3f), with ages

Tectonics
10.1029/2022TC007344

Table 1
Summary of Geochronological and Thermochronological Data From the Western Cordillera (Ecuador)

Sample	Rock	Location[a]		Elevation (m)	Zircon U-Pb age ± error (1σ) (Ma)	AFT central age ± error (1σ) (Ma)	MTL[b] ± error (1σ) (1 s.e.)[c] (μm)	Mean corrected ZHe age[d] ± error (1σ) (SD) (Ma)	Mean corrected AHe age[d] ± error (1σ) (SD) (Ma)
		Longitude (°W)	Latitude (°N)						
Chaucha profile									
EC18-06	Granodiorite	−79.51231	−2.88948	683	22.7 ± 0.5	17.6 ± 1.4	14.01 ± 0.19	12.5 ± 2.3	6.9 ± 1.9
EC18-07	Granodiorite	−79.46452	−2.90889	1181	-	11.8 ± 1.5	13.19 ± 1.23[e]	6.5 ± 0.6	4.0 ± 0.5
EC18-08	Granodiorite	−79.44443	−2.91737	1430	-	10.8 ± 1.6	14.22 ± 0.75[e]	-	5.3 ± 0.9
EC18-09	Granodiorite	−79.43179	−2.90928	1757	-	8.1 ± 1.3	15.51 ± 0.30[e]	-	5.6 ± 0.5
EC18-10	Granodiorite	−79.40974	−2.90101	1952	-	11.7 ± 1.1	14.71 ± 0.38[e]	7.6 ± 0.2	6.5 ± 1.7
EC18-11	Granodiorite	−79.37827	−2.90181	2578	16.9 ± 0.4	8.39 ± 2.0	-	-	7.4 ± 0.7
Guaranda profile									
EC18-13	Granodiorite	−79.05064	−1.49738	3063	-	-	-	-	11.7 ± 0.4
EC18-14	Granodiorite	−79.06044	−1.48916	2916	-	17.5 ± 9.0	-	-	8.5 ± 0.2[f]
EC18-15	Granodiorite	−79.07859	−1.49603	2687	-	21.7 ± 1.6	15.19 ± 0.18	-	12.5 ± 0.4
EC18-16	Granodiorite	−79.0964	−1.50065	2398	-	18.9 ± 2.0	15.29 ± 0.26	-	10.9 ± 1.4
EC18-17	Granodiorite	−79.12827	−1.51321	2086	21 ± 0.6	21.2 ± 2.3	15.10 ± 0.29	11.6 ± 2.6	11.6 ± 1.3
EC18-18	Microgranodiorite	−79.30893	−1.52260	377	-	-	-	22.8 ± 0.8	12.8 ± 3.2
EC18-19	Microgranodiorite (dyke)	−79.10582	−1.50282	2207	-	19.4 ± 1.9	14.43 ± 0.21[e]	-	-
EC18-20	Granodiorite	−79.08302	−1.49780	2575	-	21.3 ± 3.4	-	14.6 ± 1.0	9.8 ± 1.5
Apuela profile									
EC18-33	Granodiorite	−78.50474	0.37188	1852	-	17.8 ± 2.5	14.11 ± 0.32	-	4.0 ± 0.1[f]
EC18-34	Granodiorite	−78.50755	0.36715	1676	15.4 ± 0.5	15.2 ± 1.3	14.11 ± 0.25	-	4.3 ± 0.7
EC18-35	Granodiorite	−78.51672	0.35327	1514	-	18.2 ± 1.8	13.82 ± 0.19	10.2 ± 1.6	4.5 ± 1.0
EC18-36	Granodiorite	−78.58428	0.26629	1281	-	18.0 ± 1.9	13.68 ± 0.28	-	3.9 ± 0.2
EC18-37	Granodiorite	−78.62444	0.21750	987	23.9 ± 0.7	16.3 ± 1.4	14.12 ± 0.21	10.1 ± 2.8	3.8 ± 1.3
EC18-38	Granodiorite	−78.61693	0.23112	1177	-	14.3 ± 1.6	14.10 ± 0.19	-	4.7 ± 0.3
EC18-39	Granodiorite	−78.52919	0.43077	1974	-	16.7 ± 1.4	14.03 ± 0.20	-	5.2 ± 0.6
EC18-40	Granodiorite	−78.55608	0.40733	2100	-	18.7 ± 2.0	13.77 ± 0.65[e]	7.9 ± 0.3	7.3 ± 0.3

[a] Longitude and latitude coordinates are given in WGS 84 (degrees). [b] MTL is the mean track length. [c] Standard error. [d] Corrected age is the age corrected by the grain geometry and ejection factor FT (Ketcham et al., 2011). [e] Samples with less than 10 measured track lengths. [f] The mean value correspond to a single grain AHe age.

ranging from 8.7 ± 0.1 Ma to 2.3 ± 0.1 Ma. AHe single grain ages from the Guaranda area show higher inter-sample grain-age dispersion without a clear trend with changing elevation (Figure 3e). In this area, most samples are located at higher elevation, and AHe ages are dispersed around 12 Ma. ZHe ages increase with elevation at the scale of the Western Cordillera.

4.3. Thermal Modeling

Thermal histories predicted by QTQt satisfactorily reproduced AHe and AFT data for each profile (Figure 4). The ZHe thermochronometer has a wide range of temperature sensitivity depending on the radiation damage of the zircons (e.g., Ault et al., 2019). As our ZHe data show no clear correlation between the single-grain ages and eU (Figures S5–S7 in Supporting Information S1), we were not able to reproduce the measured ZHe ages with the diffusion model included in QTQt (i.e., Guenthner et al., 2013), thus the ZHe data were excluded from the thermal modeling.

The thermal histories that best predict the AHe and AFT data from inversion of the three age-elevation profiles indicate rapid cooling immediately after the emplacement of the intrusions (~100°C/Myr); followed by residence of the samples at temperatures of ~100°C from 15 to 6 Ma for the northern profile and from 11 to 6 Ma for the southern profile. The final cooling phase of the overall thermal history initiated between ~6 and 5 Ma, and continues to the present-day (~15°C/Myr). Although the Guaranda profile exhibits a similar early phase of cooling, the older, high-elevation AHe ages cannot resolve the late Miocene thermal history.

5. Discussion

5.1. Late Miocene Rock Uplift and Exhumation in the Western Ecuadorian Andes

Thermochronological and geochronological data from the Western Cordillera of Ecuador indicate a phase of rapid cooling after early Miocene crystallization of the granitic intrusions (Figure 4). This rapid cooling likely corresponds to post-magmatic cooling via thermal relaxation of the intrusions (e.g., Murray et al., 2019), although

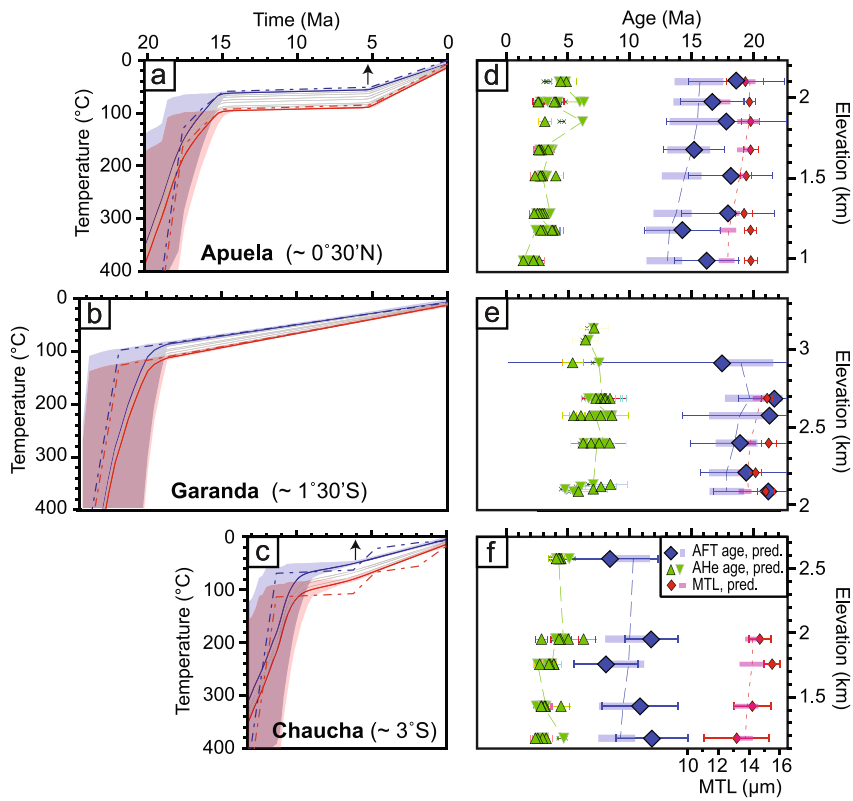

Figure 4. (a–c): t-T path for each profile. Each line represents the t-T path of a sample, the red and blue lines show the t-T path of the lower and upper sample, respectively; transparent shading indicates uncertainties. The red and blue-dashed lines denote thermal paths that fit the data best. (d–f): Age-elevation profiles for the Apuela, Guaranda, and Chaucha areas showing AFT ages, mean-track length (MTL), and AHe ages; ages predicted based on thermal history are shown by pastel colors.

coeval, tectonically controlled exhumation cannot be entirely excluded. The most recent cooling histories revealed by the Chaucha and the Apuela profiles are consistent and record an isothermal phase followed by a second cooling starting at ~6–5 Ma. The isothermal phase suggests that little exhumation occurred in the Western Cordillera between 15 and 6–5 Ma. The second cooling phase in the Western Cordillera is synchronous with the onset of the last cooling phase recorded in the Eastern Cordillera (starting at 5.5 Ma; Spikings & Crowhurst, 2004; Spikings et al., 2010), and with rapid cooling in the Coastal Cordillera between 6 and 5 Ma (Brichau et al., 2021). This late Miocene cooling phase in both ranges is also contemporaneous with the onset of alluvial-fan deposition in the basins to the west and east of the Andes (e.g., Alvarado et al., 2016), supporting the notion that cooling was associated with erosional exhumation of a growing topography. The cooling rate and the geothermal gradient of 30°C/km derived from the modeling of our thermochronological data suggest exhumation rates of ~0.5 km/Myr for the last 6 Myr, with total exhumation of ~3 km achieved since 6 Ma.

Previous thermochronological studies from the Eastern Cordillera and the Coastal Cordillera have suggested multiple phases of exhumation starting at 15, 9, and 6 Ma, and at 6 and 2 Ma, respectively (Brichau et al., 2021; Spikings et al., 2010). AFT data from the inter-Andean Cuenca Basin indicate that the region experienced a cooling history similar to that of the Eastern Cordillera, including a major cooling event at 9 Ma that was accompanied by shortening (Steinmann et al., 1999). Our new thermochronological data helps clarify the exhumation history of the Ecuadorian Andes. The AHe ages along the Guaranda and Chaucha cross sections are younger in the hanging wall of the reverse faults, whereas they are older in both the footwall and at high elevations in the hanging wall (Figures 2e and 2f). This AHe age pattern suggests rock uplift of the hanging walls of the Montalvo and Ponce Enríquez reverse faults and internal deformation of the North Andean Sliver. Thermal histories obtained for vertical profiles (Figure 4) and spatial age patterns suggest that shortening along these faults controlled uplift and exhumation in the Western Cordillera during the late Miocene, synchronous with shear-zone reactivation in the Western Cordillera (Spikings et al., 2005), and deformation and exhumation along the Eastern Cordillera and the sub-Andean ranges (Spikings & Crowhurst, 2004; Spikings et al., 2010).

Coltorti and Ollier (2000) suggested that an extensive low-relief surface in the Western Cordillera at 3,500 m was at sea level during the early Pliocene (~5.3 Ma), and became dissected due to surface uplift during the middle to late Pliocene. Together with our new thermochronological data, these geomorphologic constraints indicate a total of 3 km of exhumation in the Western Cordillera that was probably associated with rock and surface uplift and coeval erosion starting at ~6 Ma. In southern Ecuador, a low surface elevation in the Western Cordillera prior to 6 Ma is compatible with the presence of marine sediments in the inter-Andean basins that were deposited between 15 and 9 Ma (Hungerbühler et al., 2002; Steinmann et al., 1999). Considering that the combination of sedimentological and thermochronological data from the Western Cordillera and the Eastern Cordillera (i.e., Winkler et al., 2005) suggests limited structural uplift in the Western Cordillera prior to 6 Ma, we propose that the present-day topography of the Ecuadorian Andes, which includes two parallel, high-elevation mountain ranges separated by an intermontane depression, started to develop at ~6 Ma, although a volcanic arc clearly predated this phase. Interestingly, late Miocene shortening and exhumation in the Western Cordillera is consistent with recently obtained paleomagnetic data indicating a clockwise rotation of the western Ecuadorian Andes with respect to the South America during the last 10 Myr (Siravo et al., 2021).

5.2. Implications for the Timing of Carnegie Ridge Subduction

The subduction of bathymetric highs has been suggested to trigger widespread deformation and uplift at subduction margins (e.g., Dominguez et al., 1998; George et al., 2023; Lallemand et al., 1992; Ramos, 2005; Rosenbaum & Mo, 2011; von Huene et al., 1997). In addition, the subduction of oceanic aseismic ridges also appears to cause changes in the geochemical composition of magmatism with a shift to a more juvenile isotope signal in magmas (Chiaradia et al., 2020). Our thermochronological data from the Western Cordillera in Ecuador clearly document the onset of a regional uplift and exhumation phase that started between ~6 and 5 Ma (Figure 4). Our data furthermore suggest that the Ponce Enríquez and Montalvo reverse faults are major structures controlling rock uplift and exhumation in the Western Cordillera. Importantly, these faults appear to be associated with transpression and the extrusion of the North Andean Sliver along the dextral Puna-Pallatanga-Cosanga-Chingal strike-slip fault. Although motion of the North Andean Sliver may have initiated as early as 15 Ma due to oblique subduction (e.g., Alvarado et al., 2016), the Pliocene to early Pleistocene acceleration of northward motion of this block suggests increased coupling at the plate interface after the initiation of the Carnegie Ridge subduction under the South American continent (Deniaud, 1999; Witt et al., 2006). Moreover, earlier cooling and exhumation phases

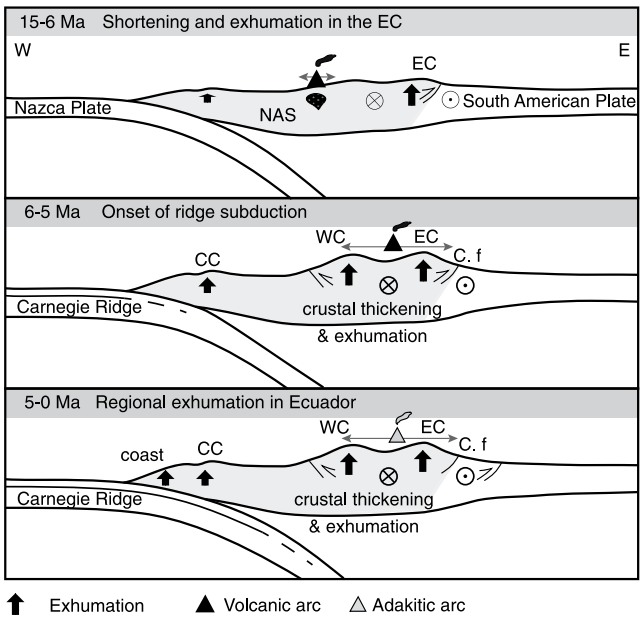

Figure 5. Schematic cross sections showing tectonic changes and topographic growth in Ecuador (at ~2°S) during the late Cenozoic. The North Andean Sliver (NAS) is highlighted in gray. The Coastal Cordillera (CC), Western Cordillera (WC), the Eastern Cordillera (EC), and the position of the magmatic arc (after George et al., 2021) are shown.

identified in the Eastern Cordillera and the Coastal Cordillera between 15 and 7 Ma (Brichau et al., 2021; Spikings et al., 2005, 2010) that have been associated with subduction of the Carnegie Ridge (i.e., Spikings et al., 2010), were synchronous with deformation and uplift recorded at 17–15, 13, and 9–8 Ma in the sub-Andean ranges of northern Peru (e.g., Mégard, 1984; Moreno et al., 2020; Sébrier et al., 1988). Notably, these earlier cooling phases are not recorded in the Western Cordillera of Ecuador, suggesting that earlier uplift and exhumation in other parts of Ecuador were independent from the subduction processes associated with the Carnegie Ridge.

The interpretation of initial Carnegie Ridge subduction starting at ~6–5 Ma is consistent with geodynamic reconstructions, the offshore morphology, and subsidence history of the Gulf of Guayaquil. Based on these studies, the onset of Carnegie Ridge subduction has been placed between 5 and ~1.8 Ma (e.g., Collot et al., 2019; Witt et al., 2006). This is also compatible with the timing of regional compressional tectonic inversion of the forearc (Daly, 1989). Furthermore, an eastward shift of volcanism between 6 and 5 Ma in northern Ecuador (Barberi et al., 1988) and an accompanying change in magma chemistry also supports a ridge-related influence on upper-plate processes at this time (e.g., Bourdon et al., 2003; Samaniego et al., 2010). For example, Hafnium isotopic compositions of zircons in Ecuador become more juvenile between 8 and 6 Ma (George et al., 2021) and indicate changes in volcanic-arc geochemistry at that time, possibly reflecting the arrival of the Carnegie Ridge at the subduction zone. In summary, the integration of new and published thermochronological and geochronological data from the Ecuadorian Andes suggests that the subduction of the Carnegie Ridge triggered shortening and exhumation as well as a variety of related structural and magmatic phenomena starting between ~6 and 5 Ma (Figure 5).

5.3. Aseismic-Ridge Subduction, Deformation, and Rock Uplift

The thermochronological data from the Ecuadorian Andes indicate that aseismic Carnegie Ridge subduction promoted Mio-Pliocene compressional deformation of the North Andean Sliver coeval with strike-slip faulting along the Puna-Pallatanga-Cosangua-Chingal fault system (e.g., Alvarado et al., 2016). We demonstrate that the oblique subduction of the Carnegie Ridge promoted regional uplift and exhumation of the Ecuadorian Andes over a timespan of several million years. The onset of tectonic uplift and exhumation is synchronous across the Ecuadorian Andes. This may be the consequence of the reactivation of pre-existing crustal heterogeneities involving strike-slip faults that facilitated the transfer and localization of deformation as well as the ensuing exhumation processes in the upper plate.

Other sectors along the South American plate margin and the North Pacific show a similar influence of subducting bathymetric anomalies on upper-plate deformation styles. For example, the oblique subduction of the Yakutat oceanic plateau in the North Pacific at ~30 Ma promoted transpressional deformation along the Denali fault system and sustained rapid exhumation in the Alaska Range (e.g., Trop et al., 2019; Waldien et al., 2022). Along the South American margin, the Chile Rise has been acting as an indenter promoting northward motion and exhumation of the Chiloe block along the Liquiñe Ofqui dextral fault zone since the late Miocene (e.g., Astudillo-Sotomayor et al., 2021; Cembrano et al., 2002; Forsythe & Nelson, 1985; Georgieva et al., 2016). In Costa Rica, the subduction of the aseismic Cocos Ridge was associated with the growth of a bivergent orogenic wedge and localized rock uplift (Morell et al., 2012). In northern Peru similar processes have taken place: Miocene uplift and exhumation of the Western Cordillera and contemporaneous deformation of the sub-Andean ranges was associated with the onset of subduction of the Nazca Ridge and subsequent slab flattening (George et al., 2023; Margirier et al., 2015). The Nazca Ridge is furthermore suggested to promote localized shortening in the overriding plate in southern Peru (Sébrier et al., 1988). Accordingly, during the Quaternary the Nazca Ridge has been responsible for the uplift of marine terraces along the Peruvian coast (Hagen & Moberly, 1994; Hsu, 1992; Macharé & Ortlieb, 1992; Regard et al., 2021; Saillard et al., 2011). Finally, the formation of the Fitzcarrald Arch in the Peruvian back-arc during the Quaternary has been associated with the southward-migrating

subduction of the Nazca Ridge (Espurt et al., 2007, 2010; Regard et al., 2009), which is thought to be linked with basal shear and thickening of the lower crust (Bishop et al., 2018). Hence, the initial subduction of bathymetric highs can lead to deformation at the margin, but also hundreds of kilometers inboard if inherited zones of crustal weakness exist.

6. Conclusions

The exhumation history of the Andean highlands of Ecuador provides a record of shortening and uplift intimately related to the subduction of the aseismic Carnegie Ridge. Our new geochronological and thermochronological data constrain several cooling phases in the Western Cordillera of Ecuador. AFT ages record cooling associated with post-magmatic thermal relaxation of early and middle Miocene intrusions. This suggests that the AFT thermochronometer is not well suited to decipher the exhumation history of the Miocene magmatic arc in the northern Andes. A second phase of cooling related to exhumation was started at ∼6–5 Ma in the Western Cordillera. Late Miocene onset of exhumation correlates closely with the onset of active shortening and rock uplift, as well as with coeval exhumation previously identified in the Coastal Cordillera and the Eastern Cordillera. We propose that the onset of regional shortening and exhumation at ∼6–5 Ma was triggered by an increase of plate coupling at the subduction interface related to the onset of the subduction of the aseismic Carnegie Ridge.

Data Availability Statement

The data is available in the table, supporting information files and can also be accessed in the Zenodo Repository (https://zenodo.org/record/7311529#Y4YTYYLMITU).

Acknowledgments
This study was supported by a PRIME grant of the German Academic Exchange Service (DAAD) to A.M., funds from the Graduate School of Potsdam University, and support from the Arizona LaserChron Center (NSF-EAR 1649254). M.S. and I.C. were supported by funds from Potsdam University and Yachay Tech University, Ecuador, provided during a visiting professorship. We thank U. Chowdhury and students for assistance at the ANGL laboratory. We appreciate valuable comments by J. Jara-Muñoz on an earlier version of the manuscript. We thank J.A. Benowitz, the anonymous reviewers, and associate editor L. Giambiagi for their thorough reviews and recommendations that helped to improve this manuscript. Open Access funding enabled and organized by Projekt DEAL.

References

Alvarado, A., Audin, L., Nocquet, J.-M., Jaillard, E., Mothes, P., Jarrin, P., et al. (2016). Partitioning of oblique convergence in the Northern Andes subduction zone: Migration history and the present-day boundary of the North Andean Sliver in Ecuador. *Tectonics*, *35*(5), 1048–1065. https://doi.org/10.1002/(ISSN)1944-9194

Armijo, R., Lacassin, R., Coudurier-Curveur, A., & Carrizo, D. (2015). Coupled tectonic evolution of Andean orogeny and global climate. *Earth-Science Reviews*, *143*, 1–35. https://doi.org/10.1016/j.earscirev.2015.01.005

Astudillo-Sotomayor, L., Jara-Muñoz, J., Melnick, D., Cortés-Aranda, J., Tassara, A., & Strecker, M. R. (2021). Fast Holocene slip and localized strain along the Liquiñe-Ofqui strike-slip fault system, Chile. *Scientific Reports*, *11*(1), 1–10. https://doi.org/10.1038/s41598-021-85036-5

Ault, A. K., Gautheron, C., & King, G. E. (2019). Innovations in (U–Th)/He, fission track, and trapped charge thermochronometry with applications to earthquakes, weathering, surface-mantle connections, and the growth and decay of mountains. *Tectonics*, *38*(11), 3705–3739. https://doi.org/10.1029/2018TC005312

Axen, G. J., van Wijk, J. W., & Currie, C. A. (2018). Basal continental mantle lithosphere displaced by flat-slab subduction. *Nature Geoscience*, *11*(12), 961–964. https://doi.org/10.1038/s41561-018-0263-9

Baby, P., Rivadeneira, M., Barragán, R., & Christophoul, F. (2013). Thick-skinned tectonics in the Oriente foreland basin of Ecuador. *Geological Society, London, Special Publications*, *377*(1), 59–76. https://doi.org/10.1785/gssrl.67.6.27

Baize, S., Audin, L., Winter, T., Alvarado, A., Moreno, L. P., Taipe, M., et al. (2015). Paleoseismology and tectonic geomorphology of the Pallatanga fault (Central Ecuador), a major structure of the South-American crust. *Geomorphology*, *237*, 14–28. https://doi.org/10.1016/j.geomorph.2014.02.030

Barberi, F., Coltelli, M., Ferrara, G., Innocenti, F., Navarro, J. M., & Santacroce, R. (1988). Plio-quaternary volcanism in Ecuador. *Geological Magazine*, *125*(1), 1–14. https://doi.org/10.1017/s0016756800009328

Bishop, B. T., Beck, S. L., Zandt, G., Wagner, L. S., Long, M. D., & Tavera, H. (2018). Foreland uplift during flat subduction: Insights from the Peruvian Andes and Fitzcarrald Arch. *Tectonophysics*, *731*, 73–84. https://doi.org/10.1016/j.tecto.2018.03.005

Bookhagen, B., & Strecker, M. R. (2008). Orographic barriers, high-resolution TRMM rainfall, and relief variations along the eastern Andes. *Geophysical Research Letters*, *35*, 6. https://doi.org/10.1029/2007gl032011

Bourdon, E., Eissen, J.-P., Gutscher, M.-A., Monzier, M., Hall, M. L., & Cotten, J. (2003). Magmatic response to early aseismic ridge subduction: The Ecuadorian margin case (South America). *Earth and Planetary Science Letters*, *205*(3), 123–138. https://doi.org/10.1016/s0012-821x(02)01024-5

Brichau, S., Reyes, P., Gautheron, C., Hernández, M., Michaud, F., Leisen, M., et al. (2021). First timing constraints on the Ecuadorian Coastal Cordillera exhumation: Geodynamic implications. *Journal of South American Earth Sciences*, *105*, 103007. https://doi.org/10.1016/j.jsames.2020.103007

Cantalamessa, G., & Di Celma, C. (2004). Origin and chronology of Pleistocene marine terraces of Isla de la Plata and of flat, gently dipping surfaces of the southern coast of Cabo San Lorenzo (Manabı, Ecuador). *Journal of South American Earth Sciences*, *16*(8), 633–648. https://doi.org/10.1016/j.jsames.2003.12.007

Capaldi, T. N., Horton, B. K., McKenzie, N. R., Mackaman-Lofland, C., Stockli, D. F., Ortiz, G., & Alvarado, P. (2020). Neogene retroarc foreland basin evolution, sediment provenance, and magmatism in response to flat slab subduction, western Argentina. *Tectonics*, *39*(7), e2019TC005958. https://doi.org/10.1029/2019tc005958

Cembrano, J., Lavenu, A., Reynolds, P., Arancibia, G., López, G., & Sanhueza, A. (2002). Late Cenozoic transpressional ductile deformation north of the Nazca–South America–Antarctica triple junction. *Tectonophysics*, *354*(3–4), 289–314. https://doi.org/10.1016/s0040-1951(02)00388-8

Chiaradia, M., Müntener, O., & Beate, B. (2020). Effects of aseismic ridge subduction on the geochemistry of frontal arc magmas. *Earth and Planetary Science Letters*, *531*, 115984. https://doi.org/10.1016/j.epsl.2019.115984

Chlieh, M., Mothes, P. A., Nocquet, J. M., Jarrin, P., Charvis, P., Cisneros, D., et al. (2014). Distribution of discrete seismic asperities and aseismic slip along the Ecuadorian megathrust. *Earth and Planetary Science Letters*, *400*, 292–301. https://doi.org/10.1016/j.epsl.2014.05.027

Collot, J.-Y., Ratzov, G., Silva, P., Proust, J. N., Migeon, S., Hernández, M. J., et al. (2019). The Esmeraldas Canyon: A helpful marker of the Pliocene-Pleistocene tectonic deformation of the north Ecuador-Southwest Colombia convergent margin. *Tectonics*, *38*(8), 3140–3166. https://doi.org/10.1190/1.9781560801580

Coltorti, M., & Ollier, C. D. (2000). Geomorphic and tectonic evolution of the Ecuadorian Andes. *Geomorphology*, *32*(1–2), 1–19. https://doi.org/10.1016/s0169-555x(99)00036-7

Daly, M. C. (1989). Correlations between Nazca/Farallon Plate kinematics and forearc evolution in Ecuador. *Tectonics*, *8*(4), 769–790. https://doi.org/10.1029/tc008i004p00769

Das, S., & Watts, A. B. (2009). Effect of subducting seafloor topography on the rupture characteristics of great subduction zone earthquakes. In *Subduction zone geodynamics* (pp. 103–118). Springer.

Dávila, F. M., Lithgow-Bertelloni, C., & Giménez, M. (2010). Tectonic and dynamic controls on the topography and subsidence of the Argentine Pampas: The role of the flat slab. *Earth and Planetary Science Letters*, *295*(1–2), 187–194. https://doi.org/10.1016/j.epsl.2010.03.039

Deniaud, Y. (1999). *Enregistrements sédimentaire et structural de l'évolution géodynamique des Andes Equatoriennes au cours du Néogène: Étude des bassins d'avant-arc et bilans de masse, Géologie Alpine, Mémoire H.S, 32* (p. 157). Université Joseph Fourier Grenoble.

Dominguez, S., Lallemand, S. E., Malavieille, J., & von Huene, R. (1998). Upper plate deformation associated with seamount subduction. *Tectonophysics*, *293*(3–4), 207–224. https://doi.org/10.1016/s0040-1951(98)00086-9

Dominguez, S., Malavieille, J., & Lallemand, S. E. (2000). Deformation of accretionary wedges in response to seamount subduction: Insights from sandbox experiments. *Tectonics*, *19*(1), 182–196. https://doi.org/10.1029/1999tc900055

Dumont, J. F., Santana, E., & Vilema, W. (2005). Morphologic evidence of active motion of the Zambapala fault, Gulf of Guayaquil (Ecuador). *Geomorphology*, *65*(3–4), 223–239. https://doi.org/10.1016/j.geomorph.2004.09.003

Eakin, C. M., Lithgow-Bertelloni, C., & Dávila, F. M. (2014). Influence of Peruvian flat-subduction dynamics on the evolution of western Amazonia. *Earth and Planetary Science Letters*, *404*, 250–260. https://doi.org/10.1016/j.epsl.2014.07.027

Egbue, O., & Kellogg, J. (2010). Pleistocene to present North Andean "escape". *Tectonophysics*, *489*(1–4), 248–257. https://doi.org/10.1016/j.tecto.2010.04.021

Ego, F. (1995). Accommodation de la convergence oblique dans une chaîne de type cordilleraine: les Andes d'Equateur (Doctoral dissertation, Paris 11).

Eguez, A., Alvarado, A., Yepes, H., Machette, M. N., Costa, C., Dart, R. L., & Bradley, L.-A. (2003). *Database and map of Quaternary faults and folds of Ecuador and its offshore regions: Open-file report 03-289*. U.S. Geological Survey.

England, P., & Molnar, P. (1990). Surface uplift, uplift of rocks, and exhumation of rocks. *Geology*, *18*(12), 1173–1177. https://doi.org/10.1130/0091-7613(1990)018<1173:suuora>2.3.co;2

Espurt, N., Baby, P., Brusset, S., Roddaz, M., Hermoza, W., & Barbarand, J. (2010). The Nazca Ridge and uplift of the Fitzcarrald Arch: Implications for regional geology in northern South America. In *Amazonia: Landscape and species evolution: A look into the past* (pp. 89–100). Wiley-Blackwell.

Espurt, N., Baby, P., Brusset, S., Roddaz, M., Hermoza, W., Regard, V., et al. (2007). How does the Nazca Ridge subduction influence the modern Amazonian foreland basin? *Geology*, *35*(6), 515. https://doi.org/10.1130/G23237A.1

Flórez-Rodríguez, A. G., Schellart, W. P., & Strak, V. (2019). Impact of aseismic ridges on subduction systems: Insights from analog modeling. *Journal of Geophysical Research: Solid Earth*, *124*(6), 5951–5969. https://doi.org/10.1029/2019jb017488

Forsythe, R., & Nelson, E. (1985). Geological manifestations of ridge collision: Evidence from the Golfo de Penas-Taitao basin, southern Chile. *Tectonics*, *4*(5), 477–495. https://doi.org/10.1029/tc004i005p00477

Freisleben, R., Jara-Muñoz, J., Melnick, D., Martínez, J. M., & Strecker, M. R. (2021). Marine terraces of the last interglacial period along the Pacific coast of South America (1°N–40°S). *Earth System Science Data*, *13*(6), 2487–2513. https://doi.org/10.5194/essd-13-2487-2021

Gallagher, K. (2012). Transdimensional inverse thermal history modeling for quantitative thermochronology. *Journal of Geophysical Research*, *117*(B2), B02408. https://doi.org/10.1029/2011jb008825

Gardner, T. W., Verdonck, D., Pinter, N. M., Slingerland, R., Furlong, K. P., Bullard, T. F., & Wells, S. G. (1992). Quaternary uplift astride the aseismic Cocos ridge, Pacific coast, Costa Rica. *The Geological Society of America Bulletin*, *104*(2), 219–232. https://doi.org/10.1130/0016-7606(1992)104<0219:quatac>2.3.co;2

Geist, E. L., Fisher, M. A., & Scholl, D. W. (1993). Large-scale deformation associated with ridge subduction. *Geophysical Journal International*, *115*(2), 344–366. https://doi.org/10.1111/j.1365-246x.1993.tb01191.x

George, S. W. M., Horton, B. K., Vallejo, C., Jackson, L. J., & Gabriela Gutierrez, E. (2021). Did accretion of the Caribbean oceanic plateau drive rapid crustal thickening in the northern Andes? *Geology*, *49*(8), 936–940. https://doi.org/10.1130/g48509.1

George, S. W. M., Perez, N. D., Struble, W., Curry, M. E., & Horton, B. K. (2023). Aseismic ridge subduction focused late Cenozoic exhumation above the Peruvian flat slab. *Earth and Planetary Science Letters*, *600*, 117754. https://doi.org/10.1016/j.epsl.2022.117754

Georgieva, V., Melnick, D., Schildgen, T. F., Ehlers, T. A., Lagabrielle, Y., Enkelmann, E., & Strecker, M. R. (2016). Tectonic control on rock uplift, exhumation, and topography above an oceanic ridge collision: Southern Patagonian Andes (47°S), Chile. *Tectonics*, *35*(6), 1317–1341. https://doi.org/10.1002/2016tc004120

Gérault, M., Husson, L., Miller, M. S., & Humphreys, E. D. (2015). Flat-slab subduction, topography, and mantle dynamics in southwestern Mexico. *Tectonics*, *34*(9), 1892–1909. https://doi.org/10.1002/2015tc003908

Gerya, T. V., Fossati, D., Cantieni, C., & Seward, D. (2009). Dynamic effects of aseismic ridge subduction: Numerical modelling. *European Journal of Mineralogy*, *21*(3), 649–661. https://doi.org/10.1127/0935-1221/2009/0021-1931

Giambiagi, L., Mescua, J., Bechis, F., Tassara, A., & Hoke, G. (2012). Thrust belts of the southern Central Andes: Along-strike variations in shortening, topography, crustal geometry, and denudation. *GSA Bulletin*, *124*(7–8), 1339–1351. https://doi.org/10.1130/b30609.1

Global Volcanism Program. (2022). *(Database) volcanoes of the World (v. 5.0.0; 1 Nov 2022)*. Distributed by Smithsonian Institution, compiled by Venzke, E. https://doi.org/10.5479/si.GVP.VOTW5-2022.5.0

Guenthner, W. R., Reiners, P. W., Ketcham, R. A., Nasdala, L., & Giester, G. (2013). Helium diffusion in natural zircon: Radiation damage, anisotropy, and the interpretation of zircon (U-Th)/He thermochronology. *American Journal of Science*, *313*(3), 145–198. https://doi.org/10.2475/03.2013.01

Gutscher, M. A., Malavieille, J., Lallemand, S., & Collot, J.-Y. (1999). Tectonic segmentation of the North Andean margin: Impact of the Carnegie Ridge collision. *Earth and Planetary Science Letters*, *168*(3), 255–270. https://doi.org/10.1016/s0012-821x(99)00060-6

Hagen, R. A., & Moberly, R. (1994). Tectonic effects of a subducting aseismic ridge: The subduction of the Nazca Ridge at the Peru Trench. *Marine Geophysical Researches*, *16*(2), 145–161. https://doi.org/10.1007/bf01224757

Hernández, M. J., Michaud, F., Collot, J. Y., Proust, J. N., & d'Acremont, E. (2020). Evolution of the Ecuador offshore nonaccretionary-type forearc basin and margin segmentation. *Tectonophysics*, *781*, 228374. https://doi.org/10.1016/j.tecto.2020.228374

Horton, B. K., Capaldi, T. N., & Perez, N. D. (2022). The role of flat slab subduction, ridge subduction, and tectonic inheritance in Andean deformation. *Geology*, *50*(9), 1007–1012. https://doi.org/10.1130/g50094.1

Horton, B. K., & Fuentes, F. (2016). Sedimentary record of plate coupling and decoupling during growth of the Andes. *Geology*, *44*(8), 647–650. https://doi.org/10.1130/g37918.1

Hsu, J. T. (1992). Quaternary uplift of the Peruvian coast related to the subduction of the Nazca Ridge: 13.5 to 15.6 degrees south latitude. *Quaternary International*, *15*, 87–97. https://doi.org/10.1016/1040-6182(92)90038-4

Hungerbühler, D., Steinmann, M., Winkler, W., Seward, D., Egüez, A., Peterson, D. E., et al. (2002). Neogene stratigraphy and Andean geodynamics of southern Ecuador. *Earth-Science Reviews*, *57*(1–2), 75–124. https://doi.org/10.1016/s0012-8252(01)00071-x

Isacks, B. L. (1988). Uplift of the central Andean plateau and bending of the Bolivian orocline. *Journal of Geophysical Research*, *93*(B4), 3211–3231. https://doi.org/10.1029/jb093ib04p03211

Jaillard, E., Guillier, B., Bonnardot, M.-A., Hassani, R., Lapierre, H., & Toro, J. (2005). Orogenic buildup of the Ecuadorian Andes. In *6th International symposium on Andean geodynamics (Barcelona), extended abstract* (pp. 404–407).

Jaillard, E., Ordonez, M., Suárez, J., Toro, J., Iza, D., & Lugo, W. (2004). Stratigraphy of the late Cretaceous–Paleogene deposits of the Cordillera Occidental of central Ecuador: Geodynamic implications. *Journal of South American Earth Sciences*, *17*(1), 49–58. https://doi.org/10.1016/j.jsames.2004.05.003

Jordán, T. E., Isacks, B. L., Allmendinger, R. W., Brewer, J. A., Ramos, V. A., & Ando, C. J. (1983). Andean tectonics related to geometry of subducted Nazca plate. *The Geological Society of America Bulletin*, *94*(3), 341–361. https://doi.org/10.1130/0016-7606(1983)94<341:atrtgo>2.0.co;2

Kay, S. M., Maksaev, V., Moscoso, R., Mpodozis, C., & Nasi, C. (1987). Probing the evolving Andean lithosphere: Mid-late tertiary magmatism in Chile (29°–30° 30′S) over the modern zone of subhorizontal subduction. *Journal of Geophysical Research*, *92*(B7), 6173–6189. https://doi.org/10.1029/jb092ib07p06173

Kay, S. M., & Mpodozis, C. (2002). Magmatism as a probe to the Neogene shallowing of the Nazca plate beneath the modern Chilean flat-slab. *Journal of South American Earth Sciences*, *15*(1), 39–57. https://doi.org/10.1016/s0895-9811(02)00005-6

Ketcham, R. A., Gautheron, C., & Tassan-Got, L. (2011). Accounting for long alpha-particle stopping distances in (U–Th–Sm)/He geochronology: Refinement of the baseline case. *Geochimica et Cosmochimica Acta*, *75*(24), 7779–7791. https://doi.org/10.1016/j.gca.2011.10.011

Lallemand, S. E., Malavieille, J., & Calassou, S. (1992). Effects of oceanic ridge subduction on accretionary wedges: Experimental modeling and marine observations. *Tectonics*, *11*(6), 1301–1313. https://doi.org/10.1029/92tc00637

Liu, L. (2015). The ups and downs of North America: Evaluating the role of mantle dynamic topography since the Mesozoic. *Reviews of Geophysics*, *53*(3), 1022–1049. https://doi.org/10.1002/2015rg000489

Lonsdale, P., & Klitgord, K. D. (1978). Structure and tectonic history of the eastern Panama Basin. *The Geological Society of America Bulletin*, *89*(7), 981–999. https://doi.org/10.1130/0016-7606(1978)89<981:sathot>2.0.co;2

Macharé, J., & Ortlieb, L. (1992). Plio-Quaternary vertical motions and the subduction of the Nazca Ridge, central coast of Peru. *Tectonophysics*, *205*(1–3), 97–108. https://doi.org/10.1016/0040-1951(92)90420-b

Margirier, A., Audin, L., Robert, X., Pêcher, A., & Schwartz, S. (2017). Stress field evolution above the Peruvian flat-slab (Cordillera Blanca, northern Peru). *Journal of South American Earth Sciences*, *77*, 58–69. https://doi.org/10.1016/j.jsames.2017.04.015

Margirier, A., Robert, X., Audin, L., Gautheron, C., Bernet, M., Hall, S., & Simon-Labric, T. (2015). Slab flattening, magmatism, and surface uplift in the Cordillera Occidental (northern Peru). *Geology*, *43*(11), 1031–1034. https://doi.org/10.1130/g37061.1

Martinod, J., Guillaume, B., Espurt, N., Faccenna, C., Funiciello, F., & Regard, V. (2013). Effect of aseismic ridge subduction on slab geometry and overriding plate deformation: Insights from analogue modeling. *Tectonophysics*, *588*, 39–55. https://doi.org/10.1016/j.tecto.2012.12.010

McQuarrie, N., Ehlers, T. A., Barnes, J. B., & Meade, B. (2008). Temporal variation in climate and tectonic coupling in the central Andes. *Geology*, *36*(12), 999–1002. https://doi.org/10.1130/g25124a.1

Mégard, F. (1984). The Andean orogenic period and its major structures in central and northern Peru. *Journal of the Geological Society*, *141*(5), 893–900. https://doi.org/10.1144/gsjgs.141.5.0893

Michaud, F., Witt, C., & Royer, J.-Y. (2009). Influence of the subduction of the Carnegie volcanic ridge on Ecuadorian geology: Reality and fiction. *Geological Society of America Memoir*, *204*(0), 217–228. https://doi.org/10.1130/2009.1204(10)

Morell, K. D., Kirby, E., Fisher, D. M., & Van Soest, M. (2012). Geomorphic and exhumational response of the central American volcanic arc to Cocos Ridge subduction. *Journal of Geophysical Research*, *117*, B4. https://doi.org/10.1029/2011jb008969

Moreno, F., Garzione, C. N., George, S. W., Horton, B. K., Williams, L., Jackson, L. J., et al. (2020). Coupled Andean growth and foreland basin evolution, Campanian–Cenozoic Bagua Basin, northern Peru. *Tectonics*, *39*(7), e2019TC005967. https://doi.org/10.1029/2019tc005967

Murray, K. E., Reiners, P. W., Thomson, S. N., Robert, X., & Whipple, K. X. (2019). The thermochronologic record of erosion and magmatism in the Canyonlands region of the Colorado Plateau. *American Journal of Science*, *319*(5), 339–380. https://doi.org/10.2475/05.2019.01

Nocquet, J. M., Jarrin, P., Vallée, M., Mothes, P. A., Grandin, R., Rolandone, F., et al. (2017). Supercycle at the Ecuadorian subduction zone revealed after the 2016 Pedernales earthquake. *Nature Geoscience*, *10*(2), 145–149. https://doi.org/10.1038/ngeo2864

Nocquet, J. M., Villegas-Lanza, J. C., Chlieh, M., Mothes, P. A., Rolandone, F., Jarrin, P., et al. (2014). Motion of continental slivers and creeping subduction in the northern Andes. *Nature Geoscience*, *7*(4), 287–291. https://doi.org/10.1038/ngeo2099

Nur, A., & Ben-Avraham, Z. (1981). Volcanic gaps and the consumption of aseismic ridges in South America. In D. K. La Verne, J. Dymond, E. J. Dasch, D. M. Hussong, & R. Roderick (Eds.), *GSA Memoirs: Nazca plate: Crustal formation and Andean convergence*.

Pedoja, K., Dumont, J. F., Lamothe, M., Ortlieb, L., Collot, J.-Y., Ghaleb, B., et al. (2006). Plio-Quaternary uplift of the manta Peninsula and La Plata Island and the subduction of the Carnegie Ridge, central coast of Ecuador. *Journal of South American Earth Sciences*, *22*(1–2), 1–21. https://doi.org/10.1016/j.jsames.2006.08.003

Pilger, R. H. (1981). Plate reconstructions, aseismic ridges, and low-angle subduction beneath the Andes. *The Geological Society of America Bulletin*, *92*(7), 448–456. https://doi.org/10.1130/0016-7606(1981)92<448:praral>2.0.co;2

Pilger, R. H. (1984). Cenozoic plate kinematics, subduction and magmatism: South American Andes. *Journal of the Geological Society*, *141*(5), 793–802. https://doi.org/10.1144/gsjgs.141.5.0793

Ramos, V. A. (2005). Seismic ridge subduction and topography: Foreland deformation in the Patagonian Andes. *Tectonophysics*, *399*(1–4), 73–86. https://doi.org/10.1016/j.tecto.2004.12.016

Ramos, V. A., Cristallini, E. O., & Pérez, D. J. (2002). The Pampean flat-slab of the central Andes. *Journal of South American Earth Sciences*, *15*(1), 59–78. https://doi.org/10.1016/s0895-9811(02)00006-8

Ramos, V. A., & Folguera, A. (2009). Andean flat-slab subduction through time. *Geological Society, London, Special Publications*, *327*(1), 31–54. https://doi.org/10.1144/sp327.3

Ramos, V. A., & Kay, S. M. (1992). Southern Patagonian plateau basalts and deformation: Backarc testimony of ridge collisions. *Tectonophysics*, *205*(1–3), 261–282. https://doi.org/10.1016/0040-1951(92)90430-e

Regard, V., Lagnous, R., Espurt, N., Darrozes, J., Baby, P., Roddaz, M., et al. (2009). Geomorphic evidence for recent uplift of the Fitzcarrald Arch (Peru): A response to the Nazca Ridge subduction. *Geomorphology*, *107*(3–4), 107–117. https://doi.org/10.1016/j.geomorph.2008.12.003

Regard, V., Martinod, J., Saillard, M., Carretier, S., Leanni, L., Hérail, G., et al. (2021). Late Miocene-quaternary forearc uplift in southern Peru: New insights from 10Be dates and rocky coastal sequences. *Journal of South American Earth Sciences*, *109*, 103261. https://doi.org/10.1016/j.jsames.2021.103261

Rodriguez Piceda, C., Scheck-Wenderoth, M., Cacace, M., Bott, J., & Strecker, M. R. (2022). Long-term lithospheric strength and upper-plate seismicity in the southern Central Andes, 29°–39°S. *Geochemistry, Geophysics, Geosystems*, *23*(3), e2021GC010171. https://doi.org/10.1029/2021gc010171

Rosenbaum, G., & Mo, W. (2011). Tectonic and magmatic responses to the subduction of high bathymetric relief. *Gondwana Research*, *19*(3), 571–582. https://doi.org/10.1016/j.gr.2010.10.007

Saillard, M., Hall, S. R., Audin, L., Farber, D. L., Regard, V., & Hérail, G. (2011). Andean coastal uplift and active tectonics in southern Peru: 10Be surface exposure dating of differentially uplifted marine terrace sequences (San Juan de Marcona, ∼15.4°S). *Geomorphology*, *128*(3–4), 178–190. https://doi.org/10.1016/j.geomorph.2011.01.004

Samaniego, P., Martin, H., Monzier, M., Robin, C., Fornari, M., Eissen, J. P., & Cotten, J. (2005). Temporal evolution of magmatism in the Northern volcanic zone of the Andes: The geology and petrology of Cayambe volcanic complex (Ecuador). *Journal of Petrology*, *46*(11), 2225–2252. https://doi.org/10.1093/petrology/egi053

Samaniego, P., Robin, C., Chazot, G., Bourdon, E., & Cotten, J. (2010). Evolving metasomatic agent in the Northern Andean subduction zone, deduced from magma composition of the long-lived Pichincha volcanic complex (Ecuador). *Contributions to Mineralogy and Petrology*, *160*(2), 239–260. https://doi.org/10.1007/s00410-009-0475-5

Schütt, J. M., & Whipp, D. M. (2020). Controls on continental strain partitioning above an oblique subduction zone, Northern Andes. *Tectonics*, *39*(4), 725. https://doi.org/10.1002/2015TC003941

Schütte, P., Chiaradia, M., & Beate, B. (2010). Geodynamic controls on Tertiary arc magmatism in Ecuador: Constraints from U–Pb zircon geochronology of Oligocene–Miocene intrusions and regional age distribution trends. *Tectonophysics*, *489*(1–4), 159–176. https://doi.org/10.1016/j.tecto.2010.04.015

Sébrier, M., Mercier, J. L., Macharé, J., Bonnot, D., Cabrera, J., & Blanc, J. L. (1988). The state of stress in an overriding plate situated above a flat slab: The Andes of central Peru. *Tectonics*, *7*(4), 895–928. https://doi.org/10.1029/tc007i004p00895

Singh, S. C., Hananto, N., Mukti, M., Robinson, D. P., Das, S., Chauhan, A., et al. (2011). Aseismic zone and earthquake segmentation associated with a deep subducted seamount in Sumatra. *Nature Geoscience*, *4*(5), 308–311. https://doi.org/10.1038/ngeo1119

Siravo, G., Speranza, F., Mulas, M., & Costanzo-Alvarez, V. (2021). Significance of northern Andes terrane extrusion and genesis of the interandean valley: Paleomagnetic evidence from the "Ecuadorian orocline". *Tectonics*, *40*(7), e2020TC006684. https://doi.org/10.1029/2020tc006684

Spikings, R., & Simpson, G. (2014). Rock uplift and exhumation of continental margins by the collision, accretion, and subduction of buoyant and topographically prominent oceanic crust. *Tectonics*, *33*(5), 635–655. https://doi.org/10.1002/2013tc003425

Spikings, R. A., & Crowhurst, P. V. (2004). (U-Th)/He thermochronometric constraints on the late Miocene-Pliocene tectonic development of the northern Cordillera Real and the Interandean Depression, Ecuador. *Journal of South American Earth Sciences*, *17*(4), 239–251. https://doi.org/10.1016/j.jsames.2004.07.001

Spikings, R. A., Crowhurst, P. V., Winkler, W., & Villagomez, D. (2010). Syn-and post-accretionary cooling history of the Ecuadorian Andes constrained by their in-situ and detrital thermochronometric record. *Journal of South American Earth Sciences*, *30*(3–4), 121–133. https://doi.org/10.1016/j.jsames.2010.04.002

Spikings, R. A., Seward, D., Winkler, W., & Ruiz, G. M. (2000). Low-temperature thermochronology of the northern Cordillera Real, Ecuador: Tectonic insights from zircon and apatite fission track analysis. *Tectonics*, *19*(4), 649–668. https://doi.org/10.1029/2000tc900010

Spikings, R. A., Winkler, W., Hughes, R. A., & Handler, R. (2005). Thermochronology of allochthonous terranes in Ecuador: Unravelling the accretionary and post-accretionary history of the Northern Andes. *Tectonophysics*, *399*(1–4), 195–220. https://doi.org/10.1016/j.tecto.2004.12.023

Spikings, R. A., Winkler, W., Seward, D., & Handler, R. (2001). Along-strike variations in the thermal and tectonic response of the continental Ecuadorian Andes to the collision with heterogeneous oceanic crust. *Earth and Planetary Science Letters*, *186*(1), 57–73. https://doi.org/10.1016/s0012-821x(01)00225-4

Steinmann, M., Hungerbühler, D., Seward, D., & Winkler, W. (1999). Neogene tectonic evolution and exhumation of the southern Ecuadorian Andes: A combined stratigraphy and fission-track approach. *Tectonophysics*, *307*(3–4), 255–276. https://doi.org/10.1016/s0040-1951(99)00100-6

Strecker, M. R., Alonso, R. N., Bookhagen, B., Carrapa, B., Hilley, G. E., Sobel, E. R., & Trauth, M. H. (2007). Tectonics and climate of the southern central Andes. *Annual Review of Earth and Planetary Sciences*, *35*(1), 747–787. https://doi.org/10.1146/annurev.earth.35.031306.140158

Taylor, F. W., Mann, P., Bevis, M. G., Edwards, R. L., Cheng, H., Cutler, K. B., et al. (2005). Rapid forearc uplift and subsidence caused by impinging bathymetric features: Examples from the New Hebrides and Solomon arcs. *Tectonics*, *24*, 6. https://doi.org/10.1029/2004tc001650

Thomson, S. N., Brandon, M. T., Reiners, P. W., Tomkin, J. H., Vásquez, C., & Wilson, N. J. (2010). Glaciation as a destructive and constructive control on mountain building. *Nature*, *467*(7313), 313–317. https://doi.org/10.1038/nature09365

Tibaldi, A., Rovida, A., & Corazzato, C. (2007). Late Quaternary kinematics, slip-rate and segmentation of a major Cordillera-parallel transcurrent fault: The Cayambe-Afiladores-Sibundoy system, NW South America. *Journal of Structural Geology*, *29*(4), 664–680. https://doi.org/10.1016/j.jsg.2006.11.008

Trop, J. M., Benowitz, J., Cole, R. B., & O'Sullivan, P. (2019). Cretaceous to Miocene magmatism, sedimentation, and exhumation within the Alaska range suture zone: A polyphase reactivated terrane boundary. *Geosphere*, *15*(4), 1066–1101. https://doi.org/10.1130/ges02014.1

Von Huene, R., Corvalán, J., Flueh, E. R., Hinz, K., Korstgard, J., Ranero, C. R., & Weinrebe, W. (1997). Tectonic control of the subducting Juan Fernández Ridge on the Andean margin near Valparaiso, Chile. *Tectonics*, *16*(3), 474–488. https://doi.org/10.1029/96tc03703

Waldien, T. S., Lease, R. O., Roeske, S. M., Benowitz, J. A., & O'Sullivan, P. B. (2022). The role of preexisting upper plate strike-slip faults during long-lived (ca. 30 Myr) oblique flat slab subduction, southern Alaska. *Earth and Planetary Science Letters*, *577*, 117242. https://doi.org/10.1016/j.epsl.2021.117242

Winkler, W., Villagomez, D., Spikings, R., Abegglen, P., Tobler, S., & Eguez, A. (2005). The Chota basin and its significance for the inception and tectonic setting of the inter-Andean depression in Ecuador. *Journal of South American Earth Sciences*, *19*(1), 5–19. https://doi.org/10.1016/j.jsames.2004.06.006

Winter, T., Avouac, J. P., & Lavenu, A. (1993). Late Quaternary kinematics of the Pallatanga strike-slip fault (Central Ecuador) from topographic measurements of displaced morphological features. *Geophysical Journal International*, *115*(3), 905–920. https://doi.org/10.1111/j.1365-246x.1993.tb01500.x

Witt, C., & Bourgois, J. (2010). Forearc basin formation in the tectonic wake of a collision-driven, coastwise migrating crustal block: The example of the North Andean block and the extensional Gulf of Guayaquil-Tumbes Basin (Ecuador-Peru border area). *GSA Bulletin*, *122*(1–2), 89–108. https://doi.org/10.1130/B26386.1

Witt, C., Bourgois, J., Michaud, F., Ordoñez, M., Jiménez, N., & Sosson, M. (2006). Development of the Gulf of Guayaquil (Ecuador) during the Quaternary as an effect of the North Andean block tectonic escape. *Tectonics*, *25*(3), TC3017. https://doi.org/10.1029/2004tc001723

Yang, T. F., Lee, T., Chen, C. H., Cheng, S. N., Knittel, U., Punongbayan, R. S., & Rasdas, A. R. (1996). A double island arc between Taiwan and Luzon: Consequence of ridge subduction. *Tectonophysics*, *258*(1–4), 85–101. https://doi.org/10.1016/0040-1951(95)00180-8

Yepes, H., Audin, L., Alvarado, A., Beauval, C., Aguilar, J., Font, Y., & Cotton, F. (2016). A new view for the geodynamics of Ecuador: Implication in seismogenic source definition and seismic hazard assessment. *Tectonics*, *35*(5), 1249–1279. https://doi.org/10.1002/2015tc003941

References From the Supporting Information

Donelick, R. A. (1993). Apatite etching characteristics versus chemical composition. *Nuclear Tracks and Radiation Measurements*, *21*(604), 1359–0189.

Evans, N. J., Byrne, J. P., Keegan, J. T., & Dotter, L. E. (2005). Determination of uranium and thorium in zircon, apatite, and fluorite: Application to laser (U-Th)/He thermochronology. *Journal of Analytical Chemistry*, *60*(12), 1159–1165. https://doi.org/10.1007/s10809-005-0260-1

Farley, K. A., & Stockli, D. F. (2002). (U-Th)/He dating of phosphates: Apatite, monazite, and xenotime. *Reviews in Mineralogy and Geochemistry*, *48*(1), 559–577. https://doi.org/10.2138/rmg.2002.48.15

Flowers, R. M., Ketcham, R. A., Shuster, D. L., & Farley, K. A. (2009). Apatite (U–Th)/He thermochronometry using a radiation damage accumulation and annealing model. *Geochimica et Cosmochimica Acta*, *73*(8), 2347–2365. https://doi.org/10.1016/j.gca.2009.01.015

Gautheron, C., Tassan-Got, L., Barbarand, J., & Pagel, M. (2009). Effect of alpha-damage annealing on apatite (U–Th)/He thermochronology. *Chemical Geology*, *266*(3–4), 157–170. https://doi.org/10.1016/j.chemgeo.2009.06.001

Gehrels, G., & Pecha, M. (2014). Detrital zircon U-Pb geochronology and Hf isotope geochemistry of Paleozoic and Triassic passive margin strata of western North America. *Geosphere*, *10*(1), 49–65. https://doi.org/10.1130/GES00889.1

Gehrels, G. E., Valencia, V., & Ruiz, J. (2008). Enhanced precision, accuracy, efficiency, and spatial resolution of U-Pb ages by laser ablation-multicollector-inductively coupled plasma-mass spectrometry. *Geochemistry, Geophysics, Geosystems*, *9*(3), Q03017. https://doi.org/10.1029/2007GC001805

Ginster, U., Reiners, P. W., Nasdala, L., & Chanmuang, C. (2019). Annealing kinetics of radiation damage in zircon. *Geochimica et Cosmochimica Acta*, *249*, 225–246. https://doi.org/10.1016/j.gca.2019.01.033

Hurford, A. J., & Green, P. F. (1982). A users' guide to fission track dating calibration. *Earth and Planetary Science Letters*, *59*(2), 343–354. https://doi.org/10.1016/0012-821x(82)90136-4

Ketcham, R. A., Carter, A., Donelick, R. A., Barbarand, J., & Hurford, A. J. (2007). Improved modeling of fission-track annealing in apatite. *American Mineralogist*, *92*(5–6), 799–810. https://doi.org/10.2138/am.2007.2281

Laslett, G. M., Galbraith, R. F., & Green, P. F. (1994). The analysis of projected fission track lengths. *Radiation Measurements*, *23*(1), 103–123. https://doi.org/10.1016/1350-4487(94)90028-0

Ludwig, K. (2008). *User's manual for Isoplot 3.64* (Vol. 4, p. 77.). Berkeley Geochronology Center Special Publication.

Pullen, A., Ibáñez-Mejia, M., Gehrels, G. E., Giesler, D., & Pecha, M. (2018). Optimization of a laser ablation-single collector-inductively coupled plasma-mass spectrometer (Thermo Element 2) for accurate, precise, and efficient zircon U-Th-Pb geochronology. *Geochemistry, Geophysics, Geosystems*, *19*(10), 3689–3705. https://doi.org/10.1029/2018gc007889

Reiners, P. W., Spell, T. L., Nicolescu, S., & Zanetti, K. A. (2004). Zircon (U-Th)/He thermochronometry: He diffusion and comparisons with 40Ar/39Ar dating. *Geochimica et Cosmochimica Acta*, *68*(8), 1857–1887. https://doi.org/10.1016/j.gca.2003.10.021

Stacey, J. S., & Kramers, J. D. (1975). Approximation of terrestrial lead isotope evolution by a two stage model. *Earth and Planetary Science Letters*, *26*(2), 207–221. https://doi.org/10.1016/0012-821x(75)90088-6